Reese, A.; Zimmermann, T.; Proefrock, D.; Irrgeher, J.:
Extreme spatial variation of Sr, Nd and Pb isotopic signatures and 48 element mass fractions in surface sediment of the Elbe River Estuary - Suitable tracers for processes in dynamic environments?
In: Science of the Total Environment. Vol. 668 (2019) 512 - 523.
First published online by Elsevier: 27.02.2019

https://dx.doi.org/10.1016/j.scitotenv.2019.02.401

Extreme spatial variation of Sr, Nd and Pb isotopic signatures and 48 element mass fractions in surface sediment of the Elbe River Estuary - Suitable tracers for processes in dynamic environments?

Anna Reese[a,b,1], Tristan Zimmermann [a,b,1], Daniel Pröfrock[a]*, Johanna Irrgeher [a,2]

[a] Helmholtz-Zentrum Geesthacht, Institute of Coastal Research, Marine Bioanalytical Chemistry, Max-Planck Str. 1, 21502 Geesthacht, Germany

[b] Universität Hamburg, Department of Chemistry, Inorganic and Applied Chemistry, Martin-Luther-King-Platz 6, 20146 Hamburg, Germany

*corresponding author: daniel.proefrock@hzg.de

[1]These two authors contributed equally as first authors to the presented work.
[2]Present address: Montanuniversität Leoben, Department of General, Analytical and Physical Chemistry, Chair of General and Analytical Chemistry, Franz-Josef-Strasse 18, 8700 Leoben, Austria

Abstract

The Elbe River has been long considered as one of the most anthropogenically impacted rivers in Europe. Its estuary is characterized by strong tidal effects, continuous dredging and dumping of sediment, and intense ship traffic between the North Sea and the Port of Hamburg. The aim of this study was to elucidate if a combined multi-element fingerprinting and isotopic tracer approach represented a suitable tool to investigate transport and mixing processes of inorganic contaminants within a complex and highly dynamic estuarine environment.

A total of 37 surface sediment samples from the tidal Elbe were characterized in a comprehensive survey by determining the mass fractions of 48 elements and the isotopic signatures of stable Sr, Nd and Pb. Statistical data analysis resolved four discrete clusters of sampling locations in the estuary: One cluster upstream of the city of Hamburg, two clusters within the mixing zone between Hamburg and the mouth of the Elbe Estuary and one cluster in the mouth of the Estuary. River sediment entering the estuary carry significantly higher loads of metals (e.g. Cu, Zn, Sb, Cd and Pb), which are rapidly “diluted” by lower elemental mass fractions in marine sediment on a remarkably small regional scale. The cluster within the mouth of the estuary is mainly characterized by extreme isotopic variations of $n(^{208}Pb)/n(^{204}Pb)$ ranging from 38.67 ± 0.15 to 73.86 ± 0.29, beside high mass fractions of U, Th, and some rare-earth elements. Determined Pb isotope ratios are among the highest reported values for terrestrial materials.

This study indicates the general potential of combined element fingerprinting and isotope tracer approaches to elucidate processes in complex river systems. Furthermore, it represents an initial characterization of the catchment area of the Elbe River as basis for future studies on river and harbor management.

Keywords

multi-isotope approach, rare-earth elements, ICP-MS, ICP-MS/MS, MC ICP-MS, environmental analysis

1. Introduction

Research on source and origin determination, transport pathways, and fate of contaminants have become important in catchments for river and port management, in order to understand the role and the individual contribution of tributaries and specific river transects, as well as the underlying mechanisms at small scales. The Elbe River is one of the major rivers in Central Europe and plays an important economic and ecological role. The river has continuously altered its course and depth and has been considered as one of the most contaminated European rivers for a long time (Kausch, 1996).

The river originates in the Ore Mountains in the Czech Republic, passes the Czech-German border after 364.52 km and discharges after another 726.95 km through an estuary into the German North Sea (Kausch, 1996). On its way through Germany, the Elbe River passes different cities including Hamburg, where the third largest harbor in Europe is located (eurostat, 2015). The harbor represents an important industrial site attracting numerous industries e.g. energy production, mineral oil processing, metal production and processing and shipbuilding (Kausch, 1996; Simon *et al.*, 2005; Tent, 1987).

In order to accommodate growing international bulk cargo, container, and cruise ships traversing the Elbe Estuary, deepening activities started as early as in 1859. During the last century four major deepening projects expanded the depth of the main shipping lane to now 14.4 m as summarized by Kappenberg (2014).

In addition to large deepening projects, extensive ongoing maintenance activities are necessary on a daily basis to keep the river navigable. Man-made changes to the river path changed tidal currents of ebb and flood leading to a strong tidal pumping effect transporting large amounts of marine sediment upstream (Meine, 2010). In addition, during the last years, the Elbe River has experienced reduced discharge from the upstream regions due to low precipitation and long, dry summer periods. In consequence, huge quantities of sediment accumulate in the Port of Hamburg caused by low currents and deep basins (Heininger *et al.*, 2015; Kappenberg and Fanger, 2007; Wetzel *et al.*, 2013). Necessary maintenance activities are mainly achieved by dredging and relocating of up to 12.2 million m^3 of sediment per year (in 2016), corresponding to 33000 m^3 per day (HPA, 2017b; Kappenberg and Fanger, 2007).

The quality of the river sediment and water is controlled by various federal and local authorities considering organic, biological, and inorganic pollutants (e.g. (BfG, 2016; HPA, 2017a)). Furthermore, the Elbe and its pollution load have been subject to research for several years, including organic (Wetzel *et al.*, 2013), as well as inorganic (Prange *et al.*, 1997; Prange *et al.*, 2001) contaminants. Even though the elemental composition of sediment, suspended particulate matter and water have been monitored since the 1990s, data of non-traditional stable isotopes are not available for the tidal impacted course of the Elbe River (henceforth referred to as tidal Elbe). These could provide better insight into the ongoing processes. In addition, beside the classical trace metal contaminants such as Pb, Cd, Hg, Zn, Cu, and Cr. Other elements such as rare-earth elements (REE) and platinum group elements are emerging contaminants due to their increasing use in industry. Information about their presence and mass fractions of these elements is rather limited for most German river systems, so these were investigated. Thus, we hypothesized that a combined approach of elemental and isotopic tracers would be an important tool providing information on

processes influencing the contaminant load, anthropogenic impact and geochemical background conditions within an aquatic ecosystem, such as the tidal Elbe.

The isotopic abundances of Sr isotopes vary as the relative abundance of the radiogenic isotope ^{87}Sr increases by the radioactive β^--decay of ^{87}Rb ($t_{1/2} = 4.88 \cdot 10^{10}$ a). Hence, $n(^{87}Sr)/n(^{86}Sr)$[3] is a measure for the age and/or type of rocks and sediment (Brand *et al.*, 2014; de Laeter *et al.*, 2003). Isotope ratios of $n(^{87}Sr)/n(^{86}Sr)$ in terrestrial materials vary from 0.70 to 0.85 and are therefore used as powerful geochemical tracer e.g. to determine the origin of sediment (Allegre and Sutcliffe, 2008; Bentley, 2006; Voerkelius *et al.*, 2010). Since the surface geology of the Elbe River catchment within Germany is predominantly of Quaternary origin (Paluska, 1992; Pawlewicz *et al.*, 1997) isotope ratios of $n(^{87}Sr)/n(^{86}Sr)$ are generally expected to be less radiogenic. A detailed map showing the geologic provinces of Central Europe, including the catchment area of the Elbe River, is given in Pawlewicz *et al.* (1997).

Natural isotope-abundance variations of Nd result from the decay of ^{147}Sm ($t_{1/2=}1.06 \cdot 10^{11}$ a) to ^{143}Nd. The conventionally measured isotope ratio $n(^{143}Nd)/n(^{144}Nd)$ underlies significant natural variation of about 0.5114 to 0.5126 that has been used in geochronology and as geochemical tracer for decades (de Laeter *et al.*, 2003; Faure and Mensig, 2004a; Meija, 2012).

Pb is among the most frequently studied isotope systems in geochemistry (Faure and Mensig, 2004b). While ^{204}Pb is an entirely primordial nuclide, ^{206}Pb, ^{207}Pb, and ^{208}Pb are end products of the radioactive decay chains of ^{238}U ($t_{1/2} = 4.468 \cdot 10^9$ a), ^{235}U ($t_{1/2} = 7.037 \cdot 10^8$ a) and ^{232}Th ($t_{1/2} = 1.40 \cdot 10^{10}$ a), respectively (de Laeter *et al.*, 2003).

[3] IUPAC-recommended notation for SI-traceable isotope-amount ratios $r=n(^iE)/n(^jE)$, with the amount of substance n, and the isotopes ^iE and ^jE of the element E. **The notation $^iE/^jE$ (e.g. $^{87}Sr/^{86}Sr$) is commonly used interchangeably,** even though lacking information on the type of quantity (microscopic vs. macroscopic). (see also Coplen TB. Guidelines and recommended terms for expression of stable-isotope-ratio and gas-ratio measurement results. Rapid Communications in Mass Spectrometry 2011; 25: 2538-2560.)

This continuous production of radiogenic Pb isotopes results in natural isotope-abundance variations for normal material (Coplen *et al.*, 2018) of 13.8 to 64.7 for $n(^{206}Pb)/n(^{204}Pb)$, 14.5 to 21.5 for $n(^{207}Pb)/n(^{204}Pb)$, 33.3 to 81.9 for $n(^{208}Pb)/n(^{204}Pb)$, ~100 ‰ for $\delta^{207}Pb/^{206}Pb$ and ~60 ‰ for $\delta^{208}Pb/^{206}Pb$ (Brand *et al.*, 2014; Conliffe *et al.*, 2013; Roy and Négrel, 2001; Teixeira *et al.*, 2002; Zhu *et al.*, 2012).

The geolateral distribution of these elemental and isotopic tracers can be used to create elemental distribution maps and isoscapes (isotopic landscapes) that provide a valuable basis for geological and ecological studies. Isoscapes of Sr have been used for tracing origins of food (Brunner *et al.*, 2010), long term migration of animals and humans (Irrgeher *et al.*, 2010) or studying environmental matter fluxes (Capo *et al.*, 1998). Examples for Sr isoscapes of e.g. the British island, France or the Danube river system can be found in the recent literature (Evans *et al.*, 2010; Willmes *et al.*, 2014; Zitek *et al.*, 2015).

In this study, a multi-element and multi-isotope tracer approach in combination with statistical data evaluation was applied for the assessment of sources, transport pathways, and the fate of inorganic contaminants and fine sediment fractions. The proposed strategy was established for the tidal Elbe. Moreover, the approach is applied in order to fundamentally characterize the current spatial distribution and composition of the Elbe Estuary surface sediment as base-layer to address future questions related to river- and port management.

2. Materials and methods

2.1. Reagents and Standards

Preparatory laboratory work was performed in a class 10,000 clean room inside a class 100 clean bench. Type I reagent-grade water (18.2 MΩ cm) was obtained from a Milli-Q Integral water purification system equipped with a QPod-Element polishing system

(Merck-Millipore, Darmstadt, Germany). Suprapur® nitric acid (65 % *w*/*w*, Merck-Millipore) and suprapur® hydrochloric acid (30 % *w*/*w*, Merck-Millipore) were further purified by double sub-boiling in quartz stills (AHF Analysentechnik, Tübingen, Germany). Tetrafluoroboric acid (38 % *w*/*w*, Chem-Lab, Zedelgem, Belgium) was used in ultra-pure quality for sample digestion without any further purification. Polyethylene flasks, tubes, and pipette tips (VWR International, Radnor, USA), as well as perfluoroalkoxy screw cap vials (Savillex, Eden Prairie, USA) were pre-cleaned in a two-stage washing procedure using nitric acid (10 % *w*/*w* and 1 % *w*/*w* respectively).

External calibration standard solutions (all traceable to NIST standards) were prepared from custom-made multi-element standards (Inorganic Ventures, Christiansburg, USA) for quantification. Single-element standards (1 g L^{-1}) of Eu, Ir, Tl and Zr were obtained from Merck-Millipore.

The reference marine sediment GBW-07313 (National Research Centre for Certified Reference Materials, Beijing, China) and the Columbia River basalt BCR-2 (U.S. Geological Survey, Reston, USA) were used for method validation.

Certified reference materials NIST SRM 987 (highly purified $SrCO_3$, NIST, Gaithersburg, USA) and NIST SRM 981 (high purity lead metal, NIST) were used for the calibration of Sr and Pb isotopic analysis (Brand *et al.*, 2014). JNdi-1 (high purity neodymium oxide, Geological Survey of Japan, Tokyo, Japan) (Tanaka *et al.*, 2000) was used as reference material for Nd isotopic measurements.

2.2. Sampling

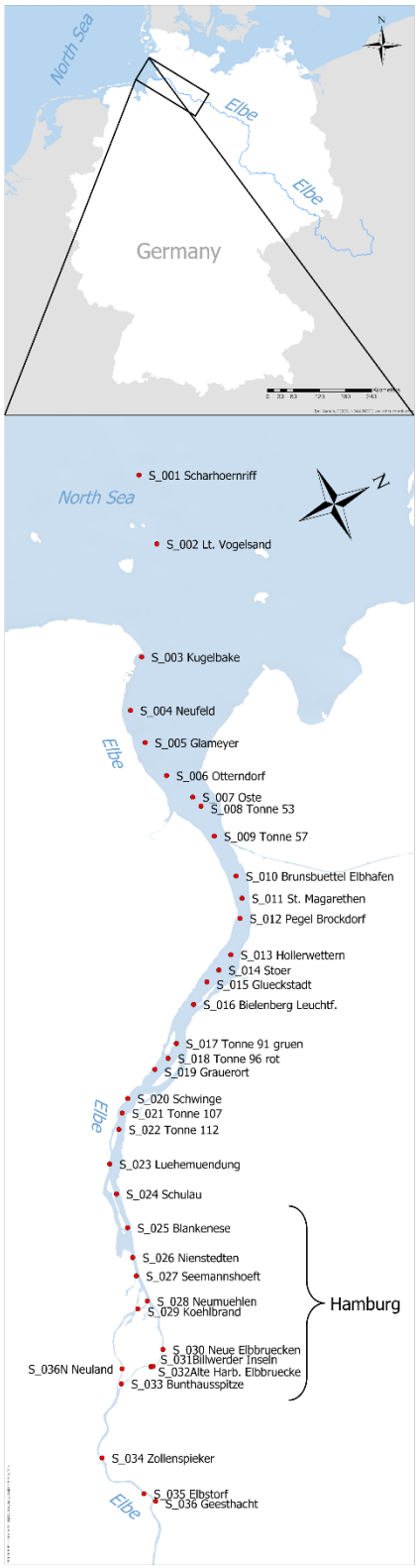

Figure 1 Map of the tidal Elbe from the weir in Geesthacht (river km 587) to the mouth into the North Sea (river km 757), passing the city of Hamburg (river km 620). The 37 sampling spots are marked as red dots. The area of Germany is shown in white, the area of all other countries in grey.

181 The surface geology of the Elbe River catchment within Germany is predominantly of
182 Quaternary origin. A detailed map showing the geologic provinces of the catchment
183 area of the River Elbe, is given in Pawlewicz *et al.* (1997).
184 A total of 37 surface sediment samples from the tidal Elbe were obtained in the course
185 of a ship sampling campaign in August 2015 from the weir of Geesthacht (river
186 kilometer 587; marking the end of the tidal impacted part of the river) to the Elbe
187 Estuary (river kilometer 757) (Figure 1). Surface sediment samples were collected
188 using a custom-made box corer. The top layer (5 to 10 cm) of three or more individual
189 samplings were subsequently homogenized and deep-frozen. A list of all samples
190 including the river kilometers and GPS coordinates is given in the Supplemental
191 Information Table A1.
192 Additionally, water samples were taken at similar sampling locations. These were
193 analyzed for pH and salinity onboard the ship, using a digital pH/conductivity meter
194 (WTW Multi 3430, WTW, Weinheim, Germany). Measured pH and salinity values can
195 be found in Supplemental Information Table A1.
196
197
198 **2.3. Sample digestion and analyte/matrix separation**
199 Homogenized sediment samples were freeze-dried (Christ Gefriertrocknungsanlagen,
200 Osterode, Germany) and sieved over a cascade of polyamide sieves (Atechnik,
201 Leinburg, Germany) to obtain the <63 µm grain size fraction. Each homogenized
202 sample was digested in triplicates by digesting about 50 mg of the sample with 5 mL
203 HNO_3, 2 mL HCl and 1 mL HBF_4 for 300 minutes at 180 °C with a MARS 5 Xpress
204 (CEM Corp., Kamp Lintfort, Germany) microwave. After digestion, the solutions were
205 transferred quantitatively to 50 mL pre-cleaned DigiTUBEs (SCP Science, Quebec,
206 Canada) and diluted to 50 mL with Milli-Q water.

The marine sediment reference material GBW-07313 and the basalt reference material BCR-2 were treated similarly. Both reference materials were quantitatively digested by the presented digestion method resulting in clear, particle free digests. Certified and measured values for the sediment certified reference material and respective recoveries for the quantified elements are given in Supplemental Information Table A2 together with the respective measurement mode of the ICP-MS/MS. Isotopic data of $n(^{87}Sr)/n(^{86}Sr)$), ($n(^{208}Pb)/n(^{204}Pb)$, $n(^{207}Pb)/n(^{204}Pb)$, $n(^{208}Pb)/n(^{206}Pb)$, $n(^{207}Pb)/n(^{206}Pb)$ and $n(^{206}Pb)/n(^{204}Pb)$ for digest replicates of both reference materials can be found in Supplemental Information Table A3.

The manual analyte/matrix separation for Sr and Pb was based on a combination of two previously published methods (Irrgeher *et al.*, 2013; Smet *et al.*, 2010). Aliquots of the digested sediment, containing 300 ng of total Pb, were transferred to a pre-cleaned 50 mL DigiTUBE, evaporated to dryness at 75 °C and re-dissolved in 3 mL of 8 mol L^{-1} HNO_3 for subsequent analyte/matrix separation. Columns were packed with 0.5 mL Sr Spec resin (SR-B-100-A, Triskem International, Bruz, France). The steps of the separation procedure, including pre-cleaning of the resin, are listed in Supplemental Information Table A4.

Separation of Nd from the sediment digest solutions was performed according to Retzmann *et al.* (2017). following an automated separation procedure using the fully automated sample preparation system prepFAST-MC® (Elemental Scientific, Omaha, USA) (Retzmann *et al.*, 2017). 10 mL aliquots of the digested samples were transferred to pre-cleaned 50 mL DigiTUBEs, evaporated to dryness at 75 °C and re-dissolved in 1 mL of 2 mol L^{-1} HNO_3 for subsequent separation. A self-packed column with 3 mL bed volume (ESI part. no. CF-3000) was utilized based on Zimmermann *et al.* (2019). The steps of the separation procedure were adapted accordingly and can also be found in Supplemental Information Table A4.

2.4. Instrumentation and measurement procedures

2.4.1. Multi-elemental analysis

Determination of elemental concentrations in the sediment digests was performed using an inductively coupled plasma tandem mass spectrometer (ICP-MS/MS) (Agilent 8800, Agilent Technologies, Tokyo, Japan) coupled to an ESI SC-4 DX FAST autosampler (Elemental Scientific, Omaha, Nebraska, USA). A list of measured isotopes and their detection modes can be found in Supplemental Information Table A2. A detailed description of all ICP-MS/MS operating parameters and used cell gas modes can be found in Supplemental Information Table A5. The instrument was tuned in a daily routine using a tune solution containing Li, Y, Ce, and Tl. Quantification was performed by external calibration, covering a concentration range from 0.1 µg L^{-1} to 100 µg L^{-1} for all analytes (10 µg L^{-1} to 10000 µg L^{-1} for Ca and P). Solutions were prepared on a daily basis from custom made multi-element standards (Inorganic Ventures, Christiansburg, USA). Wash blanks were measured after each sample triplicate to monitor potential carry over effects.

2.4.2. Isotopic analysis

A multi collector inductively coupled plasma mass spectrometer (MC ICP-MS) (Nu Plasma II, Nu Instruments Ltd, Wrexham, UK) was used for the measurement of Sr, Nd, and Pb isotope ratios. Detailed description of the instrument cup configuration and general instrumental settings of the MC ICP-MS are given in Supplemental Information Tables A6 and A7, respectively. The instrument was equipped with an APEX Q desolvation system (Elemental Scientific, Omaha, Nebraska, USA) in combination with a PFA nebulizer (Elemental Scientific, Omaha, Nebraska, USA) as sample introduction system. Daily tuning for maximum intensity, signal stability and peak shape was

accomplished by using the associated (certified) reference material (NIST SRM 987, NIST SRM 981, JNdi-1). All measurements were performed in static measurement mode with low mass resolution. Data collection was accomplished over a period of 300 s with an integration time of 10 s, resulting in 60 measurements per sample. Outlier correction was done automatically during measurement by the instrument software. Instrumental isotopic fractionation (IIF) was corrected for following an internal inter-elemental approach (combining standard sample bracketing and external calibration to account for time dependent and matrix dependent IIF variation between the samples). Isobaric interferences of residual $^{87}Rb^{+}$ on $^{87}Sr^{+}$, $^{204}Hg^{+}$ on $^{204}Pb^{+}$ and $^{144}Sm^{+}$ on $^{144}Nd^{+}$ were subtracted via peak stripping as described in chapter 2.5.2.

Separated Sr fractions were diluted to the required concentration after separation with HNO_3 (2 % *w*/*w*). The separated Pb and Nd fractions were evaporated to dryness on a hot plate at 85 °C and re-dissolved in HNO_3 (2 % *w*/*w*) prior to isotopic analysis.

Sr fractions and the corresponding isotopic standard (NIST SRM 987) were doped with Zr (Merck-Millipore) as internal standard for correction of IIF. The diluted Pb fractions and the isotopic standard (NIST SRM 981) were spiked with Tl (Merck-Millipore). Diluted Nd fractions and the isotopic standard (JNdi-1) were spiked with Eu. Concentrations of samples and bracketing standards were matched within ± 10 % in terms of the obtained signal intensities prior to analysis.

2.5. Data processing and calculations

2.5.1. Multi-elemental measurements

Multi-elemental data were processed using MassHunter version 4.2 (Agilent Technologies, Tokyo, Japan) and a custom written Excel© spreadsheet.

The Limits of Quantification (*LOD*) were calculated according to German DIN 32645 (2008) and DIN ISO 11843-2 (2006). Therefore, the *LOD* is defined as 3 x *SD* of the blank. Combined uncertainties were estimated using a Kragten spreadsheet approach (Kragten, 1994) taking into account reproducibility, repeatability, and measurement precision for selected samples. Thereafter, it was decided to report combined uncertainties as double standard deviations over triplicate digest measurements. Details about the calculation of combined uncertainty for all elements can be found in Supplemental Information B and Supplemental Information Table A8. The significant number of digits of mass fractions are given according to GUM and EURACHEM guidelines, whereby the uncertainty determines the significant number of digits to be presented with the value (Ellison and Williams, 2012; Magnusson *et al.*, 2015).

2.5.2. Isotopic measurements

Determination of absolute isotope ratio values of Sr, Nd, and Pb included on-peak baseline correction (using the *measure zeros* method of the Nu plasma software) by aspirating solutions of pure HNO_3 (2% *w*/*w*) prior to every sequence. Additional blank solutions were measured prior to every set of 5 samples. The obtained instrumental precision for e.g. $n(^{87}Sr)/n(^{86}Sr)$ was typically 6 ppm, for $n(^{208}Pb)/n(^{206}Pb)$ 20 ppm and for $n(^{143}Nd)/n(^{144}Nd)$ 3 ppm, respectively. Isobaric interferences of residual $^{87}Rb^+$ on $^{87}Sr^+$, $^{204}Hg^+$ on $^{204}Pb^+$ and $^{144}Sm^+$ on $^{144}Nd^+$ were subtracted via peak stripping as described below on the example of Sr.

As the natural fractionations of $n(^{88}Sr)/n(^{86}Sr)$ and $n(^{146}Nd)/n(^{144}Nd)$ are significant with respect to the uncertainties obtained for $n(^{87}Sr)/n(^{86}Sr)$ and $n(^{143}Nd)/n(^{144}Nd)$ after internal IIF correction, the internal intra-elemental correction approach was considered inappropriate and not applied in this study. Instead, IIF was corrected via an internal inter-elemental approach using Zr for Sr, Tl for Pb and Eu for Nd as described in detail

elsewhere (Horsky *et al.*, 2016; Irrgeher *et al.*, 2013; Irrgeher *et al.*, 2015; Kramchaninov *et al.*, 2012; Retzmann *et al.*, 2017; Yang *et al.*, 2008). A comprehensive investigation on the different calibration approaches is provided elsewhere *(Horsky et al.*, 2016; Yang *et al.*, 2018). Minor interferences of $^{87}Rb^{+}$ on $^{87}Sr^{+}$, $^{144}Sm^{+}$ on $^{144}Nd^{+}$ or $^{204}Hg^{+}$ on $^{204}Pb^{+}$ arising from residual Rb, Sm or Hg present in the purified sample solutions were mathematically corrected. As an example, this correction is described for the correction of $^{87}Rb^{+}$ on $^{87}Sr^{+}$. Herein, ^{87}Rb ($int(^{87}Rb)_{spl}$) calculated via the simultaneously measured ^{85}Rb ($int(^{85}Rb)_{spl}$) signal and using $n(^{87}Rb)/n(^{85}Rb)_{nat}$ = 0.3856 as recommended by IUPAC/CIAAW for natural Rb (Meija *et al.*, 2016b), which was corrected for IIF via sample standard bracketing (SSB) with NIST SRM 987 of known isotopic compositions ($n(^{87}Sr)/n(^{86}Sr)_{cert}$ = 0.7103426) and subsequently subtracted from ^{87}Sr ($int(^{87}Sr)_{spl}$), assuming the same IIF for $n(^{87}Sr)/n(^{86}Sr)_{spl}$ and $n(^{87}Rb)/n(^{85}Rb)_{spl}$, according to equations 1a-c:

$$int(^{87}\mathrm{Sr})_{spl} = int(87)_{spl} - int(^{85}\mathrm{Rb})_{spl} \cdot \left(\frac{n(^{87}\mathrm{Rb})}{n(^{85}\mathrm{Rb})}\right)_{nat} \cdot \left(\frac{M(^{87}\mathrm{Rb})}{M(^{85}\mathrm{Rb})}\right)^{f} \quad (1a)$$

$$f = \frac{f_{SSB_1} + f_{SSB_2}}{2} \quad (1b)$$

$$f_{SSB} = \ln\left(\frac{\left(\frac{n(^{87}\mathrm{Sr})}{n(^{86}\mathrm{Sr})}\right)_{cert}}{\left(\frac{n(^{87}\mathrm{Sr})}{n(^{86}\mathrm{Sr})}\right)_{SSB}}\right) / \ln\left(\frac{M(^{87}\mathrm{Sr})}{M(^{86}\mathrm{Sr})}\right) \quad (1c)$$

where all intensities *int* correspond to blank corrected beam intensities, $int(^{87}Sr)/int(^{86}Sr)_{SSB}$ correspond to the measured raw ratio in the SSB standard, and *M*(X) corresponds to the atomic weights according to the data from IUPAC/CIAAW tables (Meija *et al.*, 2016a).

The detailed calculation approach for Sr, Nd and Pb isotope ratio analysis and data processing including all equations and constants as well as reference values used for interference and IIF correction are given by Retzmann *et al.*(2017).

Total combined uncertainty budgets were determined for each isotopic system considering sample inhomogeneity, precision of the isotope ratio measurement for samples and standards and within-run-repeatability of the measured isotope ratio in the bracketing standards as proxy for instrument stability. Details can be found in Supplemental Information B.

2.6 Calculation of normalized REE pattern and Eu anomalies

As a proxy to calculate also possible anthropogenic influences, the REE mass fractions were normalized using the Post-Archean Australian Average Shale (PAAS). Eu-anomalies Eu/Eu* were quantified using equation 2 (McLennan, 1989).

$$\frac{\mathrm{Eu}}{\mathrm{Eu}^*} = \frac{\mathrm{Eu}_N}{(\mathrm{Sm}_N \cdot \mathrm{Gd}_N)^{0.5}} \quad (2)$$

The subscript *N* denotes PAAS-normalized mass fractions of the stated elements. If Eu is enriched relative to the other REE, a positive Eu anomaly leading to Eu/Eu*>1 is conventionally recognized. A negative Eu anomaly on the other hand gives Eu/Eu*<1.

2.7 Statistical analysis and distribution maps

Statistical evaluations were performed using STATISTICA® (StatSoft, Inc., Tulsa, USA, version 12.5). Spatial variations of the elemental and isotopic compositions were examined utilizing a hierarchical cluster analysis, using the Ward's method with Euclidean distances. A principal component analysis (PCA) was performed prior to

cluster analysis in order to identify the most determining variables for the cluster analysis.

Geographical maps showing selected parameters were created using ArcGIS® software by Esri. ArcGIS® and ArcMap™ are the intellectual property of Esri and are used herein under license.

3. Results and discussion

Sediment taken from the tidal Elbe in 2015 were analyzed for the mass fractions of 48 elements and for isotope ratios of Sr ($n(^{87}Sr)/n(^{86}Sr)$), Nd ($n(^{143}Nd)/n(^{144}Nd)$) and Pb ($n(^{208}Pb)/n(^{204}Pb)$, $n(^{207}Pb)/n(^{204}Pb)$, $n(^{208}Pb)/n(^{206}Pb)$, $n(^{207}Pb)/n(^{206}Pb)$ and $n(^{206}Pb)/n(^{204}Pb)$). All data is given with uncertainties corresponding to total combined uncertainties calculated as described in section 2.5 and Supplemental Information B with a coverage factor of k=2. Note that combined uncertainties include not only internal instrumental precision of the measured isotope ratios, but also the contribution of the blank, the correction for interferences and the repeatability of bracketing standards.

All data is provided in the Supplemental Information Table A1. Replicate data is given for three selected samples in Supplemental Information Table A9.

3.1. Statistical and regional evaluation of the tidal Elbe

PCA revealed six factors describing 93 % of the variance of the analytes along the investigated section of the tidal Elbe. The loadings of these six factors for each analyte are given in Supplemental Information Table A10.

PCA was used non-confirmatory in this study, only, in order to identify the most determining analytes as variables for the subsequent cluster analysis. However, correlations among the analytes can already be seen. Together with $n(^{208}Pb)/n(^{204}Pb)$,

the mass fractions of the REE, Ti, U, and Th correlate negatively with Factor 1. Factor 1 is also correlating with the Eu anomaly that behaves inversely to the above-mentioned analytes. Factor 2 correlates with the mass fractions of Cr, Fe, V, and Te. The mass fraction of Rb correlates with those of K, Mg, and Al that all correlate negatively with Factor 3. Factor 4 is positively correlated with the mass fractions of Zn, Sb, Cu, Cd, Ba, Pb, Tl, Bi, and Be, and negatively with the isotope ratio $n(^{207}Pb)/n(^{204}Pb)$. The isotope ratio $n(^{87}Sr)/n(^{86}Sr)$ correlates negatively with both, Factor 5 and the mass fraction of Sr. Factor 6 correlates negatively with the mass fraction of Mn.

For each of the six factors one analyte with high magnitude loadings (>|0.6|) was selected as variable for the subsequent cluster analysis. These representative analytes are the isotope ratios $n(^{208}Pb)/n(^{204}Pb)$ (Factor 1) and $n(^{87}Sr)/n(^{86}Sr)$ (Factor 5) and the mass fractions of Cr (Factor 2), Rb (Factor 3), Zn (Factor 4) and Mn (Factor 6).

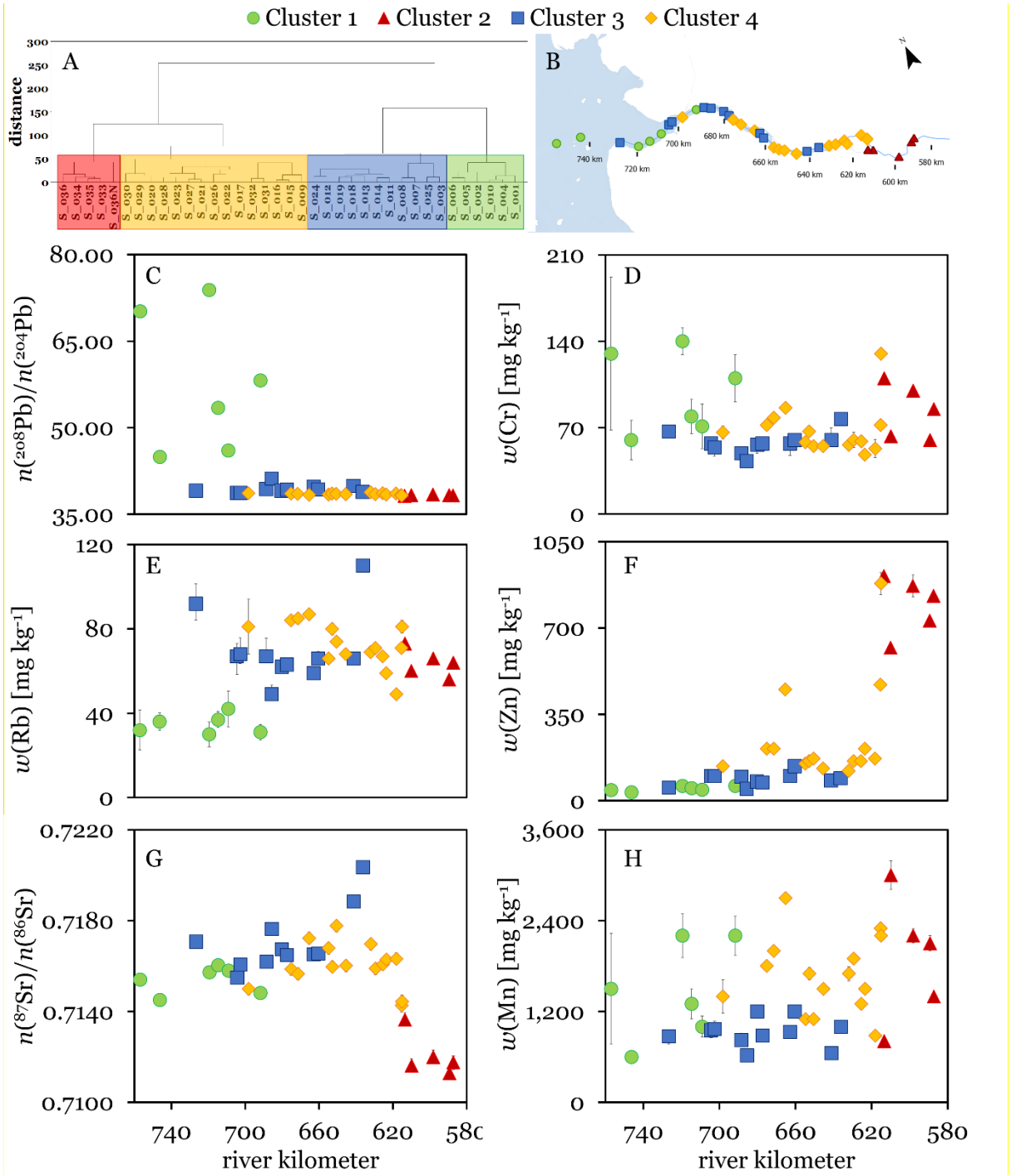

Figure 2 A) Dendrogram for the sediment samples from the tidal Elbe showing four clusters. B) Map of the tidal Elbe showing the samples with the assigned clusters color-coded. C) – H) Values of the cluster determining analytes along the tidal Elbe with the assigned clusters color-coded. Error bars correspond to expanded uncertainties *U* (*k*=2); if not visible they are in the range of spot size.

Statistical cluster analysis led to 4 statistically stable clusters within the tidal Elbe (see Figures 2A and 2B). Cluster 1 (green) is formed by six samples in the mouth of the estuary (S_001, S_002, S_004, S_005, S_006 and S_010). A geographically discrete

cluster, Cluster 2 (red), is formed by the sediment samples upstream of Hamburg, S_033 to S_036. Two larger clusters, Cluster 3 (yellow) and Cluster 4 (blue), are located between Clusters 1 and 2, overlapping and ranging from the mouth of the estuary (river kilometer 704) to the Port of Hamburg (river kilometer 615). Although Cluster 3 and Cluster 4 overlap, there is a regional trend of Cluster 3 towards the estuary mouth, while samples from Cluster 4 are generally geographically closer to Cluster 2.

Considering the six cluster determining variables (Figures 2C-2H), Cluster 1 is characterized by highly elevated values of $n(^{208}Pb)/n(^{204}Pb)$ (>44.92) and low levels of Rb (<42 mg kg^{-1}), Cluster 2 shows elevated levels of Zn (>620 mg kg^{-1}) and low values of $n(^{87}Sr)/n(^{86}Sr)$ (<0.71364). Generally, Cluster 3 and 4 show a rather similar distribution. However, in terms of Zn and its correlating elements Sb, Cu, Cd, Ba, Pb, Tl, Bi, and Be, Cluster 3 shows lower mass fractions of these elements throughout the cluster, similar to Cluster 1. In contrast, Cluster 4 shows higher levels of Zn (>120 mg kg^{-1}) and its correlating elements, especially for samples close in geographical distance to Cluster 2.

Cluster 2 upstream of Hamburg can be considered as the fluvial signal of the Elbe River entering the tidal Elbe at the weir of Geesthacht. The area covered by Clusters 3 and 4 are assumed as a mixing zone of marine and fluvial sediment, which will be discussed in the following sections. Cluster 1, however, seems to take a special position in the set of analyzed samples as the elevated values of $n(^{208}Pb)/n(^{204}Pb)$ (>44.92) (Figure 2C) are exceptionally high and accompanied by other noticeable features, as discussed below.

3.2. Strontium, neodymium and lead mass fractions and isotopic abundance ratios

Mass fractions of Sr range from 110 mg kg^{-1} to 430 mg kg^{-1} within the sediment of the tidal Elbe. The isotope ratio $n(^{87}Sr)/n(^{86}Sr)$ ranges from 0.7113 to 0.7204, representing typical values for riverine sediment (Faure and Mensig, 2004c). Figures 3A-3B show the isotope ratio $n(^{87}Sr)/n(^{86}Sr)$ and the mass fractions of Sr along the tidal Elbe.

The mass fractions of Nd range from 18 mg kg^{-1} to 650 mg kg^{-1} for the analyzed set of sediment samples. The $n(^{143}Nd)/n(^{144}Nd)$ isotope ratio varies between 0.5114 and 0.5121 as shown in Figure 3C, while the Nd mass fractions are shown in Figure 3D.

The mass fractions of Pb in the sediment of the tidal Elbe varies between 13 mg kg^{-1} and 130 mg kg^{-1}. The ratios of the Pb isotopes ranges from 38.20 to 73.86 for $n(^{208}Pb)/n(^{204}Pb)$, from 15.61 to 17.29 for $n(^{207}Pb)/n(^{204}Pb)$ and from 18.23 to 36.00 for $n(^{206}Pb)/n(^{204}Pb)$. The mass fraction of Pb and the isotope ratio values for $n(^{206}Pb)/n(^{204}Pb)$ for the Elbe sediment are shown in Figures 3E-3F. The mass fractions of Th and the isotope ratio values for $n(^{208}Pb)/n(^{204}Pb)$ are shown in Figures 3H-3G.

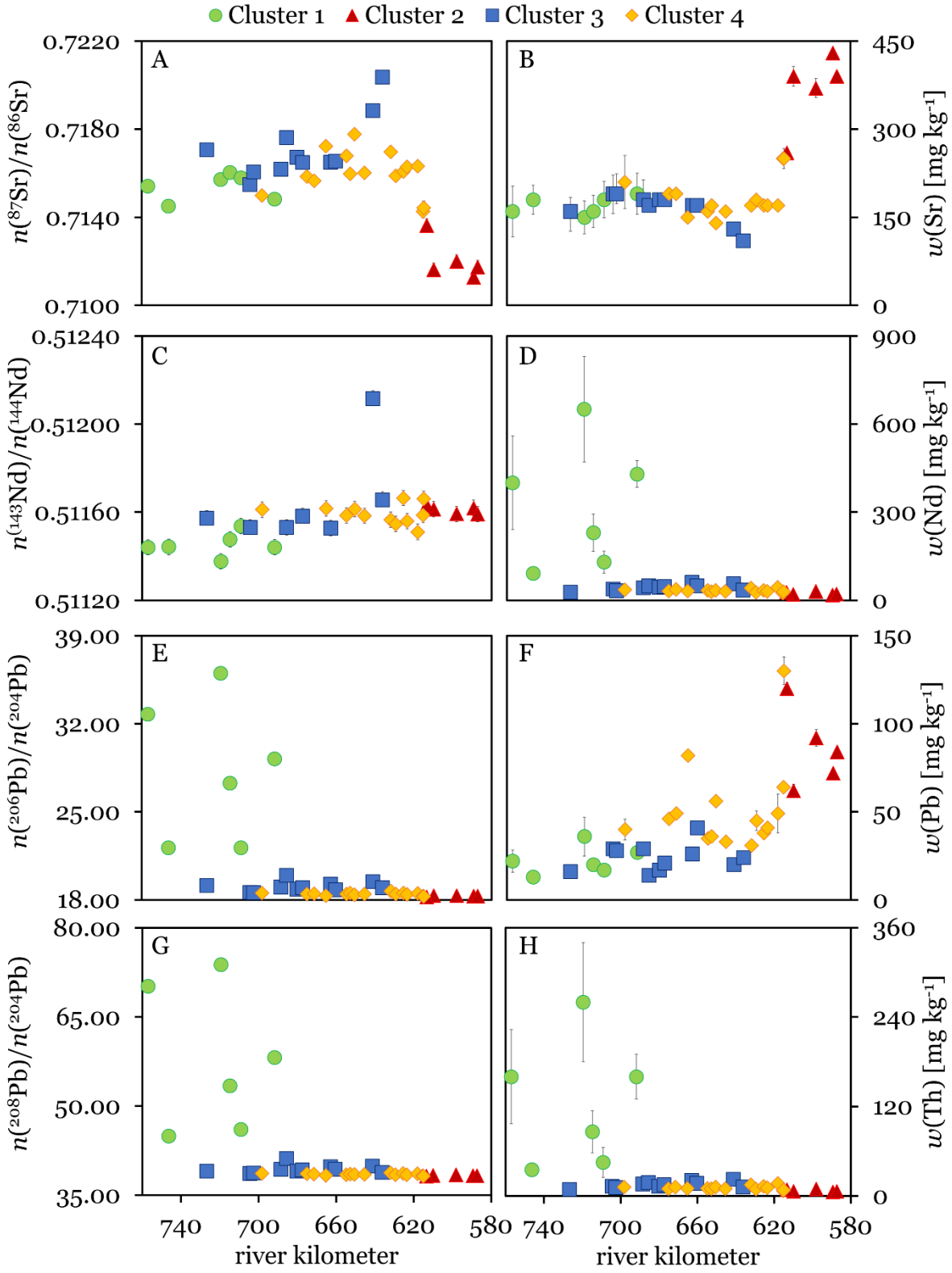

Figure 3 A) Sr isotope ratio $n(^{87}Sr)/n(^{86}Sr)$ and B) mass fraction of Sr as a function of the river kilometer C) Isotope ratio $n(^{143}Nd)/n(^{144}Nd)$ and D) mass fraction of Nd as a function of the river kilometer E) Isotope ratio $n(^{206}Pb)/n(^{204}Pb)$ and F) mass fraction of Pb vs the river kilometer G) Isotope ratio $n(^{208}Pb)/n(^{204}Pb)$ and H) mass fraction of Th vs the river kilometer. Error bars correspond to expanded uncertainties U (k=2); if not visible they are in the range of spot size.

455 The majority of the sediment samples do not exceed a value of 42 for the isotope ratio
456 $n(^{208}Pb)/n(^{204}Pb)$, with a mean value of 38.77 ± 1.23 (2*SD*). However, six sample spots
457 forming Cluster 1 show a significantly higher Pb isotopic composition (see Figure 3G):
458 S_001 (70.18 ± 0.27), S_002 (44.92 ± 0.17), S_004 (73.86 ± 0.29), S_005
459 (53.41 ± 0.21), S_006 (46.05 ± 0.18) and S_010 (58.17 ± 0.22).
460 Only few publications report Pb isotope ratios with such high amounts of radiogenic
461 lead. An extensive study by Zhu *et al.* (2012) has evaluated the majority of published
462 Pb isotopic data from 1950 to 2013. A mean value for $n(^{208}Pb)/n(^{204}Pb)$ of 38.6 ± 3.6
463 (n>5500) for terrestrial matter is reported. Published Pb isotope ratios for river
464 sediment typically range from 37.1 to 44.8 for the ratio $n(^{208}Pb)/n(^{204}Pb)$, from 15.1 to
465 17.9 for $n(^{207}Pb)/n(^{204}Pb)$ and from 17.3 to 22.5 for $n(^{206}Pb)/n(^{204}Pb)$ (Clift *et al.*, 2008;
466 Gao *et al.*, 2008; Lima *et al.*, 2005; Shepherd *et al.*, 2009). The highest
467 $n(^{208}Pb)/n(^{204}Pb)$ value for terrestrial matter ever published is 81.947 for a whole rock
468 sample from a Brazilian massif (Teixeira *et al.*, 2002).
469 Isotope ratios $n(^{208}Pb)/n(^{204}Pb)$ and $n(^{207}Pb)/n(^{204}Pb)$ do not show a correlation with
470 the mass fraction of Pb ($r(n(^{208}Pb)/n(^{204}Pb), w(Pb))$=(-0.27) and r($n(^{207}Pb)/n(^{204}Pb)$,
471 w(Pb))=(-0.28)) in the sediment samples. Moreover, when studying Figure 4C (plot of
472 $n(^{208}Pb)/n(^{204}Pb)$ versus inverse Pb mass fraction), it becomes obvious that the Pb in
473 the samples from Cluster 1 originates from a different source than the Pb in the
474 remaining samples with all samples on a mixing line between the sources. The same
475 conclusion can be drawn from the plots of $n(^{208}Pb)/n(^{204}Pb)$ against $n(^{87}Sr)/n(^{86}Sr)$ in
476 Figure 4G and $n(^{143}Nd)/n(^{144}Nd)$ against $n(^{208}Pb)/n(^{204}Pb)$ in Figure 4I.
477 However, the radiogenic Pb isotopic ratios correlate with the mass fractions of U and
478 Th ($r(n(^{208}Pb)/n(^{204}Pb), w(Th))$=0.98; $r((^{207}Pb)/n(^{204}Pb), w(U))$=0.97; $r(w(Th),$
479 w(U))=1.00). This correlation reflects the common occurrence of the radiogenic

isotopes of Pb with its mother nuclides. The correlation leads to the assumption that the extreme Pb isotope ratios originate from specific geological material.

The correlation of the isotope ratio $n(^{208}Pb)/n(^{204}Pb)$ with $n(^{206}Pb)/n(^{204}Pb)$ (r=1.00) can clearly be seen in Figure 4D. Additionally, the correlations of $n(^{208}Pb)/n(^{204}Pb)$ with the sum of the light REE (LREE) (r=0.97) and the mass fraction of Th (r=0.98) can be found in Figures 4F and 4E, respectively.

Regarding Sr and Nd the following observations were made: The $n(^{87}Sr)/n(^{86}Sr)$ isotope ratio clearly differentiates the sediment from Cluster 2 and those from the remaining clusters spatially (see Figure 3A). Cluster 2 featured significantly lower values for $n(^{87}Sr)/n(^{86}Sr)$ (<0.71364) compared to the samples downstream, indicating the border between fluvial and marine impacted sediment and the mixing zone. However, the plot of $n(^{87}Sr)/n(^{86}Sr)$ against the inverted mass fraction of Sr in Figure 4A indicated that the Sr originated from one source even though Cluster 1 seems to deviate slightly from the regression line, however, not significantly considering the uncertainties.

A similar picture is seen for Nd (Figure 4B) even though the correlation is not as pronounced as for Sr. One significant outlier was determined: S_024_Schulau from Cluster 3 has a value of $n(^{143}Nd)/n(^{144}Nd)$ = 0.51212 ± 0.00004 that is significantly higher compared to the remaining set of samples with an average value of $n(^{143}Nd)/n(^{144}Nd)$ = 0.51156 ± 0.00014 (2*SD*). Except for the Nd isotope ratio, the sampling location showed no further abnormalities.

The plot of $n(^{87}Sr)/n(^{86}Sr)$ versus $n(^{143}Nd)/n(^{144}Nd)$ (Figure 4H) shows a good separation of Clusters 1 and 2 while Clusters 3 and 4 feature comparable isotopic signatures. By combination of $n(^{87}Sr)/n(^{86}Sr)$ and $n(^{143}Nd)/n(^{144}Nd)$ a mixing process between geological younger, riverine sediment located upstream (Cluster 2) and geological older, marine sediment downstream can be observed. Detailed information

on geological and lithological background in the sampled area can be found elsewhere (Boelich and Strotmann, 2008; Paluska, 1992, Pawlewicz *et al.* 1997). Furthermore, this can be seen by the geographical intermixing of Clusters 3 and 4 (Figure 2B).

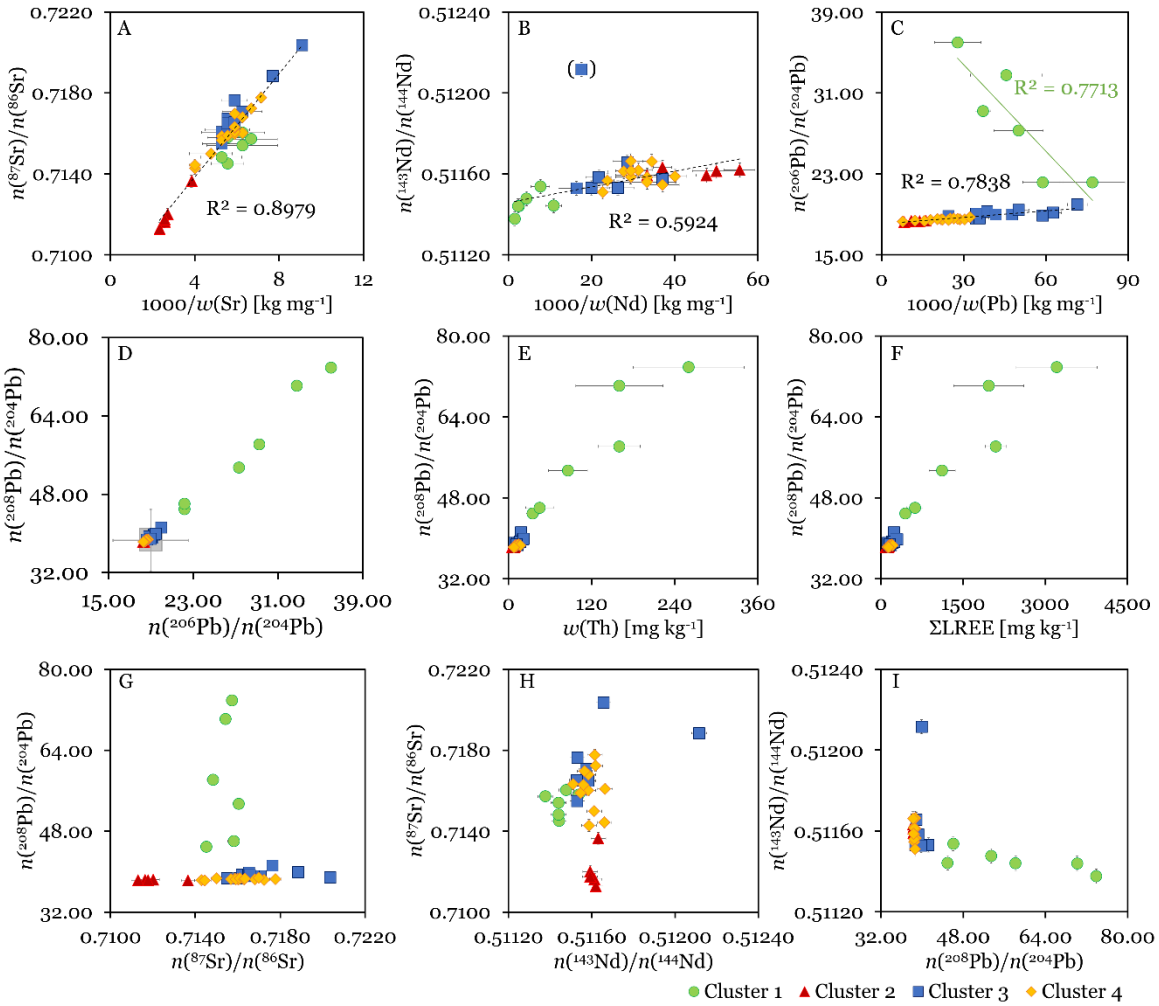

Figure 4 A) Sr isotope ratio $n(^{87}Sr)/n(^{86}Sr)$ plotted against the inverse mass fraction of Sr. B) Isotope ratio $n(^{143}Nd)/n(^{144}Nd)$ plotted against the inverse mass fraction of Nd. C) Isotope ratio $n(^{206}Pb)/n(^{204}Pb)$ plotted against the inverse mass fraction of Pb. D) The isotope ratio $n(^{208}Pb)/n(^{204}Pb)$ plotted against the ratio $n(^{206}Pb)/n(^{204}Pb)$ for the sediment of the tidal Elbe (r=1.00). The typical range of the Pb isotope ratios of terrestrial matter (Zhu and O'Nions, 1999b) is plotted in grey. E) The isotope ratio $n(^{208}Pb)/n(^{204}Pb)$ plotted against the mass fraction of Th (r=0.98). F) The isotope ratio $n(^{208}Pb)/n(^{204}Pb)$ plotted against the mass fraction of the sum of LREE (r=0.97). G) The isotope ratio $n(^{208}Pb)/n(^{204}Pb)$ plotted against $n(^{87}Sr)/n(^{86}Sr)$. H) The isotope ratio $n(^{87}Sr)/n(^{86}Sr)$ plotted against $n(^{143}Nd)/n(^{144}Nd)$. I) The isotope ratio $n(^{143}Nd)/n(^{144}Nd)$ plotted against $n(^{208}Pb)/n(^{204}Pb)$. Error bars correspond to expanded uncertainties U (k=2), if not visible they are in the range of spot size.

3.3. REE patterns

In general, all REE mass fractions show similar variations along the tidal Elbe. All REE are enriched in the samples of Cluster 1 compared to the remaining samples from the tidal Elbe. Moreover, the observed variability reflects the fluctuation of the radiogenic Pb isotopes. The ratios $n(^{208}Pb)/n(^{204}Pb)$, $n(^{207}Pb)/n(^{204}Pb)$ and $n(^{206}Pb)/n(^{204}Pb)$ show a positive correlation with increasing mass fractions of REE (r>0.95), especially of LREE (r>0.97) (see also Figure 4F).

A more detailed look at the PAAS-normalized REE patterns of all four clusters (Figures 5B to 5E) reveals differences in the REE compositions, especially in the Eu anomaly and in the ratio of LREE to heavy REE (HREE). The majority of the samples show slight Eu anomalies ranging from 0.7 to 1.1 except those from Cluster 1 (Figures 5A and 5B). All samples of Cluster 1 feature pronounced negative Eu anomalies ranging from 0.4 to 0.6. Moreover, these samples are enriched in LREE compared to HREE that becomes obvious when compared to Clusters 2, 3 and 4 (Figures 5C to 5E).

REE patterns of all analyzed samples from the tidal Elbe are typical for sediment in this area as described by Prange *et al.* (Prange *et al.* 2001) and could possibly originate from to the presence of REE-enriched heavy minerals of zircon, monazite, and allanite in this fraction. However, the large variations within small spatial distances are remarkable.

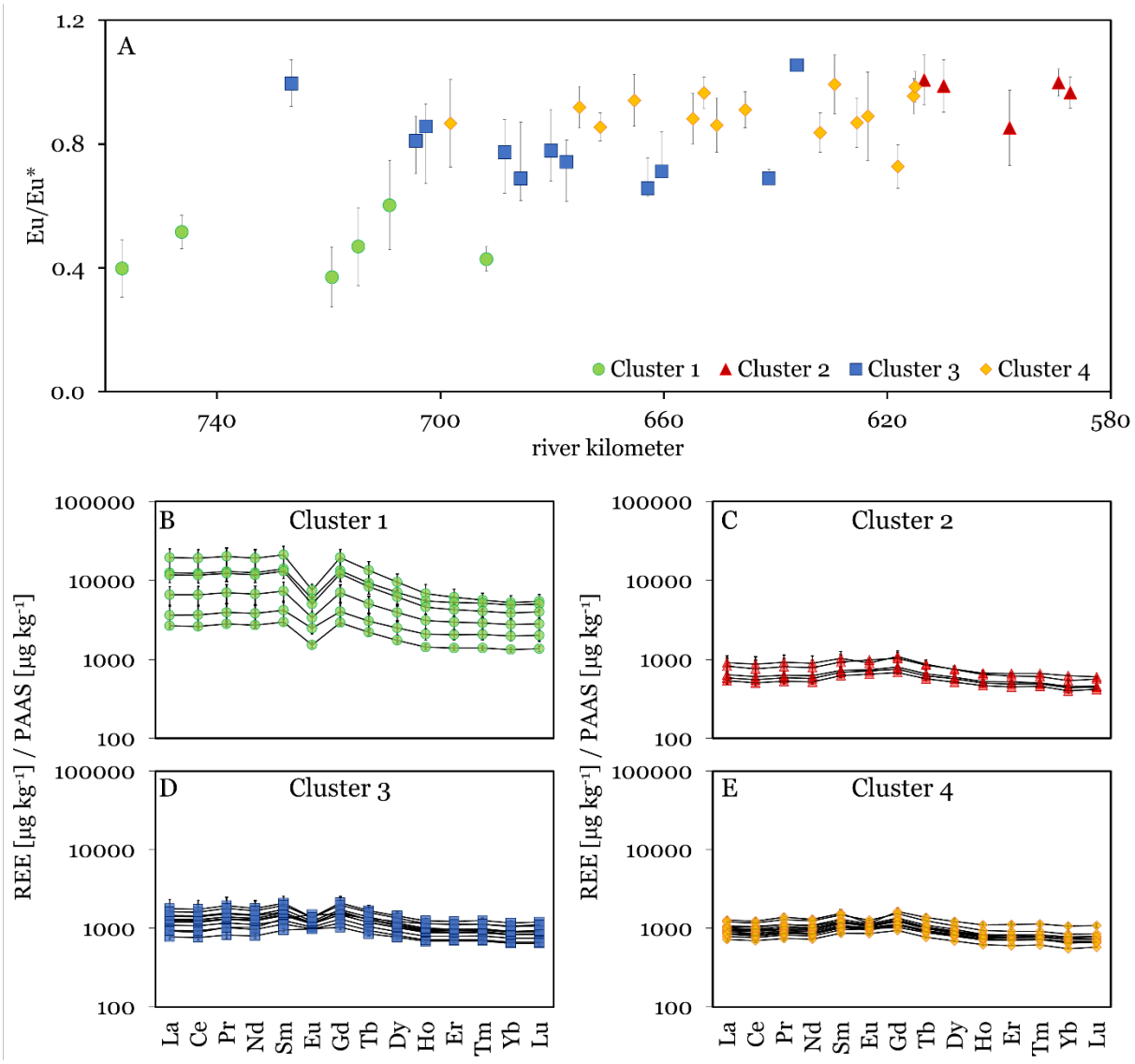

Figure 5 A) Europium anomaly as a function of the river kilometers. B) PAAS-normalized REE patterns for all samples of Cluster 1. C) PAAS-normalized REE patterns for all samples of Cluster 2. D) PAAS-normalized REE patterns for all samples of Cluster 3. E) PAAS-normalized REE patterns for all samples of Cluster 4. Error bars correspond to expanded uncertainties *U* (*k*=2).

3.4. Extreme isotopic and elemental pattern of the tidal Elbe sediment

The five samples of Cluster 2 taken upstream the Port of Hamburg (river kilometer 578 to 613) deviate significantly from all other clusters. Lower values for $n(^{87}Sr)/n(^{86}Sr)$ (<0.71364) and higher values of $n(^{143}Nd)/n(^{144}Nd)$ (>0.51159) compared to the samples downstream indicate geologically younger material at these sampling

560 locations. Additionally, mass fractions of classical metal contaminants e.g. Zn (Figure
561 2F), Sr (Figure 3B), Pb (Figure 3F), Cu and Cd (Supplemental Information Table A1)
562 are significantly higher than for Clusters 3 and 4. Assuming the origin of geological
563 younger material to be upstream the Elbe Estuary and the origin of geological older
564 material to be marine (Schoer, 1990), a rapid “dilution” of polluted riverine sediment
565 with marine sediment is suggested. This mixing of two endmembers is also supported
566 by the plot of $n(^{87}Sr)/n(^{86}Sr)$ against the inverted mass fraction of Sr in (Figure 4A) and
567 the geographical mixing of Clusters 3 and 4 (Figure 2B). Most interestingly, this mixing
568 process takes place at a very small regional scale in the City of Hamburg. As described
569 by Schoer (1990), marine sediment in the Elbe is transported upstream, caused by
570 20 % higher flood current velocities compared to ebb current velocities (“tidal
571 pumping”). The maximum upstream transport of marine sediment was estimated to be
572 located between river km 623 and 617, which is in very good agreement with the results
573 of this study.
574 The samples in Cluster 1 deviate significantly in their elemental and isotopic signatures
575 from the samples upstream. Especially, the radiogenic isotope ratios of Pb show
576 extreme values accompanied by high mass fractions of Th, U and REE. In addition,
577 high mass fractions of Ti in the range of 8800 mg kg^{-1} ± 2500 mg kg^{-1} to 40000 mg kg^{-1}
578 ± 11000 mg kg^{-1} are found for these six samples that are significantly higher than the
579 average mass fraction of the samples from Clusters 2, 3 and 4 (3400 mg kg^{-1}) (w(Ti)
580 see Supplemental Information Table A1). These extreme variations are remarkable
581 as they occur at a small spatial scale (average distance between sample spots: 5 km)
582 in a very dynamic system (strong tidal currents, permanent dredging activities,
583 shipping) and are not explainable by the underlying geology of the Elbe Estuary, which
584 is assumed to be rather uniform and young, lying above Pleistocene and Holocene
585 sediment (Boelich and Strotmann, 2008; Paluska, 1992). Hence, it can be assumed

586 that material with this distinct isotopic and elemental signature is not original to the
587 area but was transported into the Elbe Estuary either by human activities or tidal
588 dynamics as proposed by Schoer (1990).
589 Significantly different isotopic and elemental signatures were observed for samples
590 S_001, S_002, S_004, S_005, S_006 and S_010 (Cluster 1). Highly radiogenic Pb
591 isotope ratios and high mass fractions of Th, U, and REE in the grain size fraction
592 <63 µm are typical for monazite, which is a phosphate mineral with the general formula
593 [(LREE)PO_4]. Monazite is of industrial relevance as it is an important source for Th and
594 REE (Overstreet, 1967; Zhu and O'Nions, 1999a; Zhu *et al.*, 1997). The chemical
595 composition of monazites is highly variable. However, similar to samples assigned to
596 Cluster 1, monazites are typically depleted in HREE and enriched in LREE (cf. Figure
597 5B). Moreover, the enrichment of LREE in monazites correlates with the mass fractions
598 of Th and U and shows negative correlation with the mass fraction of Pb (Zhu and
599 O'Nions, 1999a; Zhu and O'Nions, 1999b). The investigated samples show a positive
600 correlation of the $n(^{208}Pb)/n(^{204}Pb)$, $n(^{207}Pb)/n(^{204}Pb)$ and $n(^{206}Pb)/n(^{204}Pb)$ ratios with
601 the mass fractions of Th and U ($r_{av}((n(^{20x})Pb/n(^{204})Pb); w(U, Th))=0.98$). The correlation
602 with the Pb mass fraction is not pronounced, but in general negative
603 ($r_{av}((n(^{20x})Pb/n(^{204})Pb); w(Pb))=-0.28$). Some studies report negative Eu anomalies for
604 monazite grains of up to 0.2 (Zhu and O'Nions, 1999a; Zhu and O'Nions, 1999b). The
605 most negative Eu anomaly in the analyzed sediment from the Elbe Estuary was
606 determined for sample S_004 with Eu/Eu*=0.37 ± 0.10 (cf. Figure 5 and Supplemental
607 Information Table A1).
608 Previously described similarities of the elemental and isotopic composition of the
609 samples from Cluster 1 with monazite indicate that the <63 µm fraction of the sediment
610 samples are enriched with monazite and/or other heavy minerals.

611 Enriched Th and U contents in sediment have also been reported earlier in the context
612 of phosphate fertilizer production and the accompanied storage and discharge of the
613 by-product phosphogypsum (Martínez-Aguirre *et al.*, 1994; Rutherford *et al.*, 1994;
614 Sanders *et al.*, 2013). Phosphogypsum is mainly composed of $CaSO_4$ x 2 H_2O
615 (gypsum) and other minor solid phases, such as phosphate, fluoride, organic matter,
616 and trace elements including natural radionuclides (Ayres *et al.*, 2011; Macías *et al.*,
617 2017; Rutherford *et al.*, 1994). The composition of phosphogypsum depends on the
618 provenance of the initial phosphate rock (Rutherford *et al.*, 1994). Moreover, elevated
619 concentrations of Th, U, Cd, Zr, and REE, as observed in samples of Cluster 1 (cf.
620 Supplemental Information Table A1), were reported in several studies on
621 phosphogypsum (de Oliveira *et al.*, 2007; Martínez-Aguirre *et al.*, 1994; Pérez-López
622 *et al.*, 2015; Rutherford *et al.*, 1994; Sanders *et al.*, 2013; Van Der Heijde *et al.*, 1990).
623 A prominent and well-studied example of high contamination from phosphogypsum is
624 the Estuary of Huelva in Spain where phosphogypsum was discharged directly into the
625 Odiel River until 1998 *(Villa et al.*, 2009). The remaining stockpiles of phosphogypsum
626 in the margins of the Estuary of Huelva are still a source of contamination for the
627 aquatic environment due to “weathering processes” (Macías *et al.*, 2017; Pérez-López
628 *et al.*, 2016; Pérez-López *et al.*, 2015). To our knowledge, the only potential source
629 that could cause phosphogypsum contamination of sediment in the Elbe Estuary are
630 two fertilizer manufacturers close to the Rhine delta. Two million tons per year of
631 phosphogypsum were discharged into the river and transported to the North Sea in the
632 1980s (Van Der Heijde *et al.*, 1990). Van der Heijde *et al.* report deposition of silt
633 containing gypsum outside the Dutch coast as far as into the German Wadden Sea
634 including amongst others the Elbe Estuary (Van Der Heijde *et al.*, 1990). The
635 previously described similarities between the elemental signature of the samples of
636 Cluster 1 and sediment samples close to phosphogypsum stockpiles and

phosphogypsum itself may lead to the conclusion that the <63 µm fraction of the sediment samples from the tidal Elbe might be contaminated by the insoluble components of phosphogypsum transported and remobilized by tidal dynamics.

This study provided the basis for source determination of sediment in the context of sediment transport within the Elbe Estuary. A deeper understanding of the processes taking place down- and upstream the harbor basin in Hamburg is essential concerning future river- and harbor management in terms of sedimentation and dredging.

4. Summary and Conclusion

Thirty-seven surface sediment samples of the tidal Elbe were characterized in a comprehensive survey by determining the mass fraction of 48 elements and isotopic signatures of Sr Nd and Pb. Statistically-significant spatial variations were found for all three isotopic systems and for the elemental data. Sediment samples were classified into four general clusters based on isotopic and elemental characteristics.

The five sampling locations of Cluster 2, located upstream the Port of Hamburg were characterized by high concentrations of metals e.g. Zn, Pb, Cu and Cd. Based on the isotopic signatures of $n(^{87}Sr)/n(^{86}Sr)$ and $n(^{143}Nd)/n(^{144}Nd)$ it is evident that riverine sediment are quickly “diluted” by marine sediment that was transported upstream by tidal currents. The majority of this mixing process takes place at a remarkable small spatial scale within a few kilometers close to the Port of Hamburg. Further, mixing of marine and riverine sediment was observed between the Port of Hamburg and the mouth of the estuary. Remarkably high variation in $n(^{208}Pb)/n(^{204}Pb)$ were found for Cluster 1 in the mouth of the estuary together with high mass fractions of REE, Th and U. Potential sources for these sediment were discussed, however, without the definite knowledge about the endmembers, these assumptions remain uncertain. The

663 determination of endmembers is especially challenging in such a dynamic system as
664 the tidal Elbe.
665 The generated dataset represents the basis for further investigation related to
666 sediment transport in the tidal Elbe. This is of particular interest for marine ecosystem
667 studies, as the mechanisms of metal “dilution” plays an important role. Furthermore,
668 port and river authorities require such datasets in order to plan and evaluate
669 relocation/dredging and disposal of sediment that is necessary to keep the river
670 navigable for large cargo ships. Stability of the findings together with time-dependent
671 changes of the seafloor in the estuary will be investigated in future sampling
672 campaigns.
673 Our results also indicate that the exclusive focus on the quantitative analysis of metal
674 contamination within the context of environmental research related to complex land-
675 river-sea systems provides only limited information. The progress achieved in isotope
676 ratio analysis of metals over the last decade opens a valuable additional dimension of
677 information.
678 Data provided gives information for source attribution of the sediment masses that are
679 transported within the Elbe River upstream to the harbor area and will allow a future
680 differentiation between upstream as well as harbor-based contaminants, which
681 strongly impact the handling (e.g. dumping vs. decontamination) of the sediment
682 masses. This may also assist with identification of responsible producers of
683 contamination, which is of utmost importance for the river and harbor management.
684

685 **Acknowledgements**

686 Ulrike Kleeberg and Linda Baldewein (HZG) are acknowledged for their support on
687 ArcGIS analysis and handling and Dr. Thilo Eichenberg (StatSoft Europe) for his
688 valuable input on statistical data analysis. We thank Kay-Christian Emeis (HZG), Urs

689 Klötzli (University of Vienna) and Xiang-Kun Zhu (Chinese Academy of Geological
690 Sciences) for fruitful discussions. Further, we would like to thank Andrea Lapschies for
691 sample preparation as well as Robert Georg Marlin Maas and Katharina Sendlhofer
692 for their support in the lab (all HZG). The anonymous reviewers are acknowledged for
693 their comments on a previous version of the manuscript.

694

695 **Competing interests declaration**

696 The authors have no competing interests to declare.
697

698 **Funding**

699 This research did not receive any specific grant from funding agencies in the public,
700 commercial, or not-for-profit sectors.

701

702 **Appendix A. Supplementary data**

703 Supplementary data associated with this article can be found in the online version, at
704 doi: https://doi.org/10.1016/j.scitotenv.2019.02.401

705

706 **References**

707 DIN ISO 11843-2:2006-06, Erkennungsfähigkeit - Teil 2: Verfahren im Fall der linearen
708 Kalibrierung (ISO 11843-2:2000; Text Deutsch, Englisch). Beuth Verlag GmbH, 2006.

709 DIN 32645:2008-11, Chemical analysis - Decision limit, detection limit and determination limit
710 under repeatability conditions - Terms, methods, evaluation. Beuth Verlag GmbH,
711 2008.

712 Allegre CJ, Sutcliffe C. Radiogenic isotope geochemistry. Isotope Geology. Cambridge
713 University Press, Cambridge, 2008, pp. 220-357.

714 Ayres RU, Holmberg J, Andersson B. Materials and the Global Environment: Waste Mining in
715 the 21st Century. MRS Bulletin 2011; 26: 477-480.

716 Bentley RA. Strontium isotopes from the earth to the archaeological skeleton: A review.
717 Journal of Archaeological Method and Theory 2006; 13: 135-187.

718 BfG. Jahresbericht 2014/2015. Bundesanstalt für Gewässerkunde, Koblenz, 2016, pp. 26.

719 Boelich MJ, Strotmann T. The Elbe Estuary. Die Küste 2008; 74: 288-306.

720 Brand WA, Coplen TB, Vogl J, Rosner M, Prohaska T. Assessment of international reference
721 materials for isotope-ratio analysis (IUPAC Technical Report). Pure and Applied
722 Chemistry 2014; 86: 425-467.

723 Brunner M, Katona R, Stefánka Z, Prohaska T. Determination of the geographical origin of
724 processed spice using multielement and isotopic pattern on the example of Szegedi
725 paprika. European Food Research and Technology 2010; 231: 623-634.

726 Capo RC, Stewart BW, Chadwick OA. Strontium isotopes as tracers of ecosystem
727 processes: theory and methods. Geoderma 1998; 82: 197-225.

728 Clift PD, Long HV, Hinton R, Ellam RM, Hannigan R, Tan MT, *et al.* Evolving east Asian river
729 systems reconstructed by trace element and Pb and Nd isotope variations in modern
730 and ancient Red River-Song Hong sediments. Geochemistry, Geophysics,
731 Geosystems 2008; 9.

732 Conliffe J, Wilton DHC, Blamey NJF, Archibald SM. Paleoproterozoic Mississippi Valley Type
733 Pb–Zn mineralization in the Ramah Group, Northern Labrador: Stable isotope, fluid
734 inclusion and quantitative fluid inclusion gas analyses. Chemical Geology 2013; 362:
735 211-223.

736 Coplen TB. Guidelines and recommended terms for expression of stable-isotope-ratio and
737 gas-ratio measurement results. Rapid Communications in Mass Spectrometry 2011;
738 25: 2538-2560.

739 Coplen TB., Holden NE, Wieser ME, Böhlke JK. Clarification of the term „normal material“
740 used for standard atomic weights (IUPAC Technical Report). Pure and Applied
741 Chemistry 2018; 90: 1221-1224.

742 de Laeter JR, Böhlke JK, De Bièvre P, Hidaka H, Peiser HS, Rosman KJR, *et al.* Atomic
743 weights of the elements. Review 2000 (IUPAC Technical Report). Pure and Applied
744 Chemistry 2003; 75: 683-800.

745 de Oliveira SMB, da Silva PSC, Mazzilli BP, Favaro DIT, Saueia CH. Rare earth elements as
746 tracers of sediment contamination by phosphogypsum in the Santos estuary,
747 southern Brazil. Applied Geochemistry 2007; 22: 837-850.

748 Ellison SLR, Williams A. Eurachem/CITAC guide: Quantifying Uncertainty in Analytical
749 Measurement, 2012.

750 eurostat. Top 20 ports - gross weight of goods handled in each port, by direction. 2018,
751 2015.

752 Evans JA, Montgomery J, Wildman G, Boulton N. Spatial variations in biosphere 87Sr/86Sr
753 in Britain. Journal of the Geological Society 2010; 167: 1-4.

754 Faure G, Mensig TM. The Oceans. Isotopes: Principles and Applications. John Wiley &
755 Sons, Hoboken, New Jersey, 2004a, pp. 436-493.

756 Faure G, Mensig TM. The U-Pb, Th-Pb, and Pb-Pb Methods. Isotopes: Principles and
757 Applications. John Wiley & Sons, Hoboken, New Jersey, 2004b, pp. 214-255.

758 Faure G, Mensig TM. Water and Sediment. Isotopes: Principles and Applications. John Wiley
759 & Sons, Hoboken, New Jersey, 2004c, pp. 412-435.

760 Gao B, Liu Y, Sun K, Liang X, Peng P, Sheng G, *et al.* Precise determination of cadmium
761 and lead isotopic compositions in river sediments. Anal Chim Acta 2008; 612: 114-
762 120.

763 Heininger P, Keller I, Quick I, Schwartz R, Vollmer S. Sediment Management on River-
764 Basinscale: The River Elbe. In: Heininger P, Cullmann J, editors. Sediment Matters.
765 Springer International Publishing Switzerland, 2015, pp. 201-247.

766 Horsky M, Irrgeher J, Prohaska T. Evaluation strategies and uncertainty calculation of
767 isotope amount ratios measured by MC ICP-MS on the example of Sr. Anal Bioanal
768 Chem 2016; 408: 351-367.

769 HPA. Teilbericht: Umlagerung von Baggergut nach Neßsand. Umgang mit Baggergut aus
770 dem Hamburger Hafen. Hamburg Port Authority, Hamburg, 2017a, pp. 40.

HPA. Umgang mit Baggergut aus dem Hamburger Hafen

Teilbericht: Umlagerung von Baggergut nach Neßsand Bericht über den Zeitraum 1.1. bis 31.12.2016. Hamburg Port Authority, Hamburg, 2017b.

Irrgeher J, Prohaska T, Sturgeon RE, Mester Z, Yang L. Determination of strontium isotope amount ratios in biological tissues using MC-ICPMS. Analytical Methods 2013; 5: 1687-1694.

Irrgeher J, Teschler-Nicola M, Leutgeb K, Weiß C, Daniela K, Prohaska T. Migration and Mobility in the Latest Neolithic of the Traisen Valley, Lower Austria − Sr Isotope Analysis. TOPOI Conference on Migrations in Prehistory and Early History, Berlin, 2010.

Irrgeher J, Vogl J, Santner J, Prohaska T. CHAPTER 8 Measurement Strategies. In: Prohaska T, Irrgeher J, Zitek A, Jakubowski N, editors. Sector Field Mass Spectrometry for Elemental and Isotopic Analysis. The Royal Society of Chemistry, 2015, pp. 126-151.

Kappenberg J. Das Elbe-Ästuar - Natürliche Entwicklung und menschliche Eingriffe. In: Ratter BMW, editor. Hamburger Symposium Geographie. 6. Institut für Geographie der Universität Hamburg, Hamburg, 2014.

Kappenberg J, Fanger H-U. Sedimenttransportgeschehen in der tidebeeinflussten Elbe, der Deutschen Bucht und in der Nordsee, Geesthacht, 2007, pp. 125.

Kausch H. Die Elbe - ein immer wieder veränderter Fluß. In: Lozán JL, Kausch H, editors. Warnsignale aus Flüssen und Ästuaren. Parey Buchverlag, Berlin, 1996.

Kragten J. Tutorial review. Calculating standard deviations and confidence intervals with a universally applicable spreadsheet technique. The Analyst 1994; 119: 2161-2165.

Kramchaninov AY, Chernyshev IV, Shatagin KN. Isotope analysis of strontium by multicollector inductively-coupled plasma mass spectrometry: High-precision combined measurement of 88Sr/86Sr and 87Sr/86Sr isotope ratios. J. Anal. Chem. 2012; 67: 1084-1092.

Lima AL, Bergquist BA, Boyle EA, Reuer MK, Dudas FO, Reddy CM, *et al.* High-resolution historical records from Pettaquamscutt River basin sediments: 2. Pb isotopes reveal a potential new stratigraphic marker. Geochimica et Cosmochimica Acta 2005; 69: 1813-1824.

Macías F, Pérez-López R, Cánovas CR, Carrero S, Cruz-Hernandez P. Environmental Assessment and Management of Phosphogypsum According to European and United States of America Regulations. Procedia Earth and Planetary Science 2017; 17: 666-669.

Magnusson B, Ellison SLR, Örnemark U. Eurachem Guide: Template for Eurachem Guides – A Guide for Editors, 2015.

Martínez-Aguirre A, García-León M, Ivanovich M. The distribution of U, Th and 226Ra derived from the phosphate fertilizer industries on an estuarine system in Southwest Spain. Journal of Environmental Radioactivity 1994; 22: 155-177.

McLennan SM. Rare earth elements in sedimentary rocks influence of provenance and sedimentary processes. Reviews in Mineralogy and Geochemistry 1989; 21: 169-200.

Meija J. Calibration of isotope amount ratios by analysis of isotope mixtures. Anal Bioanal Chem 2012; 403: 2071-2076.

Meija J, Coplen TB, Berglund M, Brand WA, De Bievre P, Groning M, *et al.* Atomic weights of the elements 2013 (IUPAC Technical Report). Pure and Applied Chemistry 2016a; 88: 265-291.

Meija J, Coplen TB, Berglund M, Brand WA, De Bievre P, Groning M, *et al.* Isotopic compositions of the elements 2013 (IUPAC Technical Report). Pure and Applied Chemistry 2016b; 88: 293-306.

Meine M. Accessibility: An Example from the River Elbe. TIDE Times 2010: 7-8.

Overstreet WC. The Geologic Occurrence Of Monazite. U.S. Geological Survey, 1967.

Paluska A. Geographie und geologische Vorgeschichte der norddeutschen Ästuare, erläutert am Beispiel der Elbe. Berichte aus dem Zentrum für Meeres- und Klimaforschung der Universitaet Hamburg 1992; 19: 1-32.

Pawlewicz MJ, Steinshouer DW, Gautier DL. Map showing geology, oil and gas fields, and geologic provinces of Europe including Turkey. Open-File Report, 1997.

Pérez-López R, Macías F, Cánovas CR, Sarmiento AM, Pérez-Moreno SM. Pollutant flows from a phosphogypsum disposal area to an estuarine environment: An insight from geochemical signatures. Science of The Total Environment 2016; 553: 42-51.

Pérez-López R, Nieto JM, de la Rosa JD, Bolívar JP. Environmental tracers for elucidating the weathering process in a phosphogypsum disposal site: Implications for restoration. Journal of Hydrology 2015; 529: 1313-1323.

Prange A, Bössow E, Erbslöh B, Jablonski R, Jantzen E, Kause P, *et al.* Zusammenfassende Aus- und Bewertung der Längsprofiluntersuchungen in der Elbe. Erfassung und Beurteilung der Belastung der Elbe mit Schafstoffe. GKSS-Forschungszentrum Geesthacht GmbH, Geesthacht, 1997.

Prange A, Bössow E, Erbslöh B, Jablonski R, Jantzen E, Kause P, *et al.* Grafische Darstellung der Längsprofile - Filtarte, Schwebstoffe, Sedimente -. Erfassung und Beurteilung der Belastung der Elbe mit Schafstoffe. GKSS-Forschungszentrum Geesthacht GmbH, Geesthacht, 2001.

Retzmann A, Zimmermann T, Pröfrock D, Prohaska T, Irrgeher J. A fully automated simultaneous single-stage separation of Sr, Pb, and Nd using DGA Resin for the isotopic analysis of marine sediments. Analytical and Bioanalytical Chemistry 409, 2017, 5463-5480.

Roy S, Négrel P. A Pb isotope and trace element study of rainwater from the Massif Central (France). Science of The Total Environment 2001; 277: 225-239.

Rutherford PM, Dudas MJ, Samek RA. Environmental impacts of phosphogypsum. Science of The Total Environment 1994; 149: 1-38.

Sanders LM, Luiz-Silva W, Machado W, Sanders CJ, Marotta H, Enrich-Prast A, *et al.* Rare Earth Element and Radionuclide Distribution in Surface Sediments Along an Estuarine System Affected by Fertilizer Industry Contamination. Water, Air, & Soil Pollution 2013; 224: 1742.

Schoer JH. Determination of the origin of suspended matter and sediments in the Elbe estuary using natural tracers. Estuaries 1990; 13: 161-172.

Shepherd TJ, Chenery SR, Pashley V, Lord RA, Ander LE, Breward N, *et al.* Regional lead isotope study of a polluted river catchment: River Wear, Northern England, UK. Science of The Total Environment 2009; 407: 4882-4893.

Simon M, Bekele V, Kulasová B, Maul C, Oppermann R, Řehák P. Die Elbe und ihr Einzugsgebiet, Magdeburg, 2005, pp. 262.

Smet I, De Muynck D, Vanhaecke F, Elburg M. From volcanic rock powder to Sr and Pb isotope ratios: a fit-for-purpose procedure for multi-collector ICP–mass spectrometric analysis. Journal of Analytical Atomic Spectrometry 2010; 25: 1025-1032.

Tanaka T, Togashi S, Kamioka H, Amakawa H, Kagami H, Hamamoto T, *et al.* JNdi-1: a neodymium isotopic reference in consistency with LaJolla neodymium. Chemical Geology 2000; 168: 279-281.

Teixeira NP, Bettencourt JS, Moura CAV, Dall'Agnol R, Macambira EMB. Archean crustal sources for Paleoproterozoic tin-mineralized granites in the Carajás Province, SSE Pará, Brazil: Pb–Pb geochronology and Nd isotope geochemistry. Precambrian Research 2002; 119: 257-275.

Tent L. Contaminated sediments in the Elbe estuary: Ecological and economic problems for the Port of Hamburg. Hydrobiologia 1987; 149: 189-199.

Van Der Heijde HB, Klijn PJ, Duursma K, Eisma D, De Groot AJ, Hagel P, et al. Environmental aspects of phosphate fertilizer production in The Netherlands: With particular reference to the disposal of phosphogypsum. Science of The Total Environment 1990; 90: 203-225.

Villa M, Mosqueda F, Hurtado S, Mantero J, Manjón G, Periañez R, *et al.* Contamination and restoration of an estuary affected by phosphogypsum releases. Science of The Total Environment 2009; 408: 69-77.

Voerkelius S, Lorenz GD, Rummel S, Quétel CR, Heiss G, Baxter M, *et al.* Strontium isotopic signatures of natural mineral waters, the reference to a simple geological map and its potential for authentication of food. Food Chemistry 2010; 118: 933-940.

Wetzel MA, Wahrendorf D-S, von der Ohe PC. Sediment pollution in the Elbe estuary and its potential toxicity at different trophic levels. Science of The Total Environment 2013; 449: 199-207.

Willmes M, McMorrow L, Kinsley L, Armstrong R, Aubert M, Eggins S, *et al.* The IRHUM (Isotopic Reconstruction of Human Migration) database – bioavailable strontium isotope ratios for geochemical fingerprinting in France 2018. Earth System Science Data, 2014.

Yang L, Peter C, Panne U, Sturgeon RE. Use of Zr for mass bias correction in strontium isotope ratio determinations using MC-ICP-MS. J. Anal. At. Spectrom. 2008; 23: 1269-1274.

Yang L, Tong S, Zhou L, Hu Z, Mester Z, Meija J. A critical review on isotopic fractionation correction methods for accurate isotope amount ratio measurements by MC-ICP-MS. Journal of Analytical Atomic Spectrometry 2018.

Zhu XK, Benefield J, Coplen TB, Hirata T, Holden NE, Prohaska T. Evaluation of published lead isotopic data (1950-2013) for a new standard atomic weight of lead. 2018, 2012.

Zhu XK, O'Nions RK. Monazite chemical composition: some implications for monazite geochronology. Contributions to Mineralogy and Petrology 1999a; 137: 351-363.

Zhu XK, O'Nions RK. Zonation of monazite in metamorphic rocks and its implications for high temperature thermochronology: a case study from the Lewisian terrain. Earth and Planetary Science Letters 1999b; 171: 209-220.

Zhu XK, ONions RK, Belshaw NS, Gibb AJ. Lewisian crustal history from in situ SIMS mineral chronometry and related metamorphic textures. Chemical Geology 1997; 136: 205-218.

Zimmermann T, Retzmann A, Schober M, Pröfrock D, Prohaska T, Irrgeher J. Matrix separation of Sr and Pb for isotopic ratio analysis of Ca-rich samples via an automated simultaneous separation procedure. Spectrochimica Acta Part B: Atomic Spectroscopy. 151, 2019, 54–64.

Zitek A, Tchaikovsky A, Irrgeher J, Waidbacher H, Prohaska T. The 87Sr/86Sr river water isoscape of the Danube catchment. In: ICPDR, editor. Joint Danube Survey 3: A

912 Comprehensive Analysis of Danube Water Quality. ICPDR, Vienna, 2015, pp. 349-
913 354.
914
915
916